A Neural Network-Based Low-Cost Solar Irradiance Sensor

Fernando Mancilla-David, *Member, IEEE*, Francesco Riganti-Fulginei, *Member, IEEE*, Antonino Laudani, *Member, IEEE*, and Alessandro Salvini, *Member, IEEE*

***Abstract*— Measuring solar irradiance allows for direct maximization of the efficiency in photovoltaic power plants. However, devices for solar irradiance sensing, such as pyranometers and pyrheliometers, are expensive and difficult to calibrate and thus seldom utilized in photovoltaic power plants. Indirect methods are instead implemented in order to maximize efficiency. This paper proposes a novel approach for solar irradiance measurement based on neural networks, which may, in turn, be used to maximize efficiency directly. An initial estimate suggests the cost of the sensor proposed herein may be price competitive with other inexpensive solutions available in the market, making the device a good candidate for large deployment in photovoltaic power plants. The proposed sensor is implemented through a photovoltaic cell, a temperature sensor, and a low-cost microcontroller. The use of a microcontroller allows for easy calibration, updates, and enhancement by simply adding code libraries. Furthermore, it can be interfaced via standard communication means with other control devices, integrated into control schemes, and remote-controlled through its embedded web server. The proposed approach is validated through experimental prototyping and compared against a commercial device.**

***Index Terms*— Neural networks, photovoltaic cells, pyranometer, sensor systems, solar irradiance.**

I. Introduction

SOLAR irradiance is a key parameter for maximum power point (MPP) tracking (MPPT) in photovoltaic (PV) power plants. This is because the operating point at which a PV array delivers its maximum power changes as a function of the solar irradiance and cell temperature. See, for example, [1]–[3] and references within. This is illustrated in Figs. 1 and 2 through typical current–voltage (I–V) curves for a PV array. Thus, if the solar irradiance and cell temperature are sensed, one could compute the MPP and directly maximize efficiency by forcing the PV array to operate at that point. The PV array's operating point is regulated by adjusting the duty cycle of the power converter connected at the output of the array. Temperature sensing is easy, however, measuring solar irradiance is difficult because irradiance sensors are expensive and difficult to calibrate [4].

Manuscript received February 27, 2013; revised June 21, 2013; accepted July 28, 2013. Date of publication October 1, 2013; date of current version February 5, 2014. The Associate Editor coordinating the review process was Dr. Amitava Chatterjee.

F. Mancilla-David is with the Department of Electrical Engineering, University of Colorado Denver, Denver, CO 80204 USA (e-mail: fernando.mancilla-david@ucdenver.edu).

F. Riganti-Fulginei, A. Laudani, and A. Salvini are with the Dipartimento di Elettronica Applicata, Università di Roma Tre, Rome 00154, Italy.

Color versions of one or more of the figures in this paper are available online at http://ieeexplore.ieee.org.

Digital Object Identifier 10.1109/TIM.2013.2282005

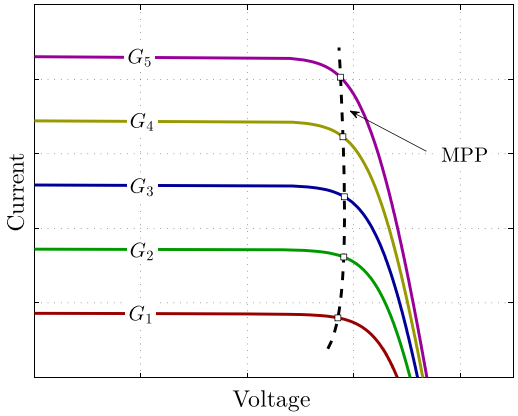

Fig. 1. Typical I–V performance curves for different irradiance values with $G_1 < G_2 < G_3 < G_4 < G_5$.

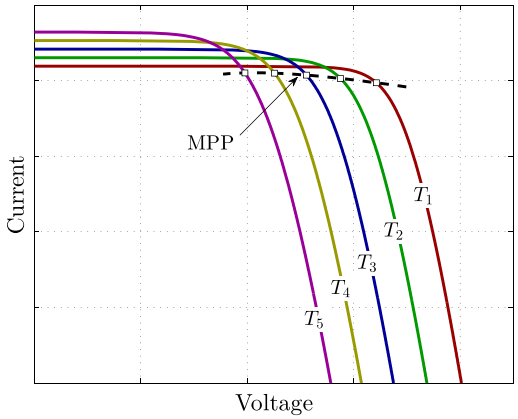

Fig. 2. Typical I–V performance curves for different cell temperature values with $T_1 < T_2 < T_3 < T_4 < T_5$.

Researchers have developed different algorithms to adjust the converter's duty cycle to perform the MPPT function, avoiding a direct measurement of solar irradiance. A class of MPPT algorithms rely on the concave shape of the PV array power–voltage curve and search for the MPP through iterative processes, without knowledge of solar irradiance. Examples of these methods include the perturb & observe (P&O) and incremental conductance algorithms [5]–[7]. These methods are not flawless, they may oscillate around the MPP and can fail under rapidly changing irradiance conditions [6]. In order to overcome these limitations, several papers have recently appeared in the literature based on neural networks (NN) [8]–[10] and on approximate solutions of the I–V curves [11].

A different approach is to predict/estimate the value of solar irradiance from the equations, which describe the PV

array model [12]–[15] and use this predicted/estimated value to perform the MPPT function.

The need for precise solar irradiance sensing stems from the fact that PV power plants usually span over a large geographical area and, as a result, the irradiance is not uniform. Known as shading effect, this adversely affects the overall efficiency of the power extraction process. Solutions include: 1) a modularization of the PV power plant in various segments using one power converter per segment with a separate MPP tracking algorithm and 2) a dynamic reconfiguration of the PV panels' interconnection with only one power converter [12]. The latter requires a precise tracking of the irradiance at various locations through the power plant, and therefore low-cost irradiance sensors are highly desirable.

It is noteworthy that irradiance tracking through remote sensing techniques could be used, in principle, to cover large power plants. However, due to the requirements of precise tracking including shades generated by small clouds, tree, and other blocking objects, a sensor in situ will yield the "ground truth" and hence may be preferred. A sensor *in situ* mounted on the PV panel can also account for the inclination of the PV panels and can generate real-time irradiance data for MPPT control algorithms.

This paper makes use of ideas developed for both MPPT and solar irradiance estimation to introduce a novel low-cost solar irradiance sensor. The approach consists of using one or a small number of PV cells together with a NN algorithm appositely tailored for the solution of an inverse problem. While the traditional approach has been to make use of NNs to track the MPP without the knowledge of the solar irradiance, the approach herein considers the implementation of a NN approach to sense the irradiance, which in turn can be also used to track the MPP.

Other authors have already proposed low-cost irradiance sensors [16], [17], but the chief advantage of the approach proposed herein lies in the simplicity of construction along with great accuracy. Furthermore, the use of a microcontroller allows for a straightforward calibration and interfacing via RS232, RS485, or Ethernet with the rest of the PV power plant control system. Microcontrollers have widely been utilized in industrial applications, but usually the algorithms used in these applications are traditional deterministic control processes. The implementation of soft computing techniques have been limited to fuzzy logic-based approaches in electric appliances [18], [19] and, recently, have been expanded to NNs in sensors for industrial applications [18], [20]–[22]. An example of usage of microcontrollers in solar irradiance data acquisition is available in [23].

Nowadays, the possibility of utilizing accurate double-precision mathematic library of efficient C compilers and integrated development environment (IDE) for code development has greatly simplified the implementation of NNs in microcontrollers. Furthermore, it has been conjectured in recent publications the "artificial intelligence" of NNs (and of other soft computing techniques) inserted in low-cost microcontrollers may lead to the design of several innovative low-cost systems for environmental sensors and controls in the near future [19], [24]. Thus, this paper takes advantage of these recent technological advancements and a low-cost microcontroller is used for the implementation.

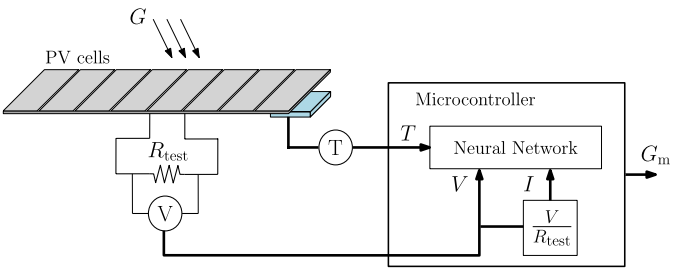

Fig. 3. Schematic of the proposed solar irradiance sensor.

The calibration may be performed utilizing the PV cell model obtained from manufacturers' datasheets or through laboratory measurements in order to avoid potential errors due to model uncertainty [25] stemming from parasitic elements or inaccuracies on datasheets [26]–[28].

The rest of this paper is organized as follows. Section II introduces the sensor architecture, followed by the NN implementation in Section III. Section IV validates the approach through experimental prototyping and comparison against a commercial sensor, and finally the conclusions follow in Section V.

II. Sensor Realization

Fig. 3 shows the overall block diagram of the approach. One or a small number of PV cells can be arranged in series/parallel in order to form a small sensing PV panel, which is connected to a known testing resistor, R_{test}. The approach consists in measuring the voltage across the cell terminals and cell temperature. Unlike solar irradiance sensing, measurement of voltage and temperature is inexpensive and easy to implement. Both of these quantities are fed into a properly trained NN algorithm implemented in a low-cost microcontroller, which computes the actual solar irradiance with great accuracy.

This sensor can be conveniently located next to a power-producing PV panel or even integrated with it. This features the advantage that the sensing PV panel will "see" exactly the same solar irradiance and temperature as that "seen" by the power-producing PV panel, leading to improved performance.

III. NN Implementation

The computation of solar irradiance through a NN has been chosen because of its versatility. Although several algorithms for multivariate fitting exist, they usually need data made on regular grids whereas NNs can perform multidimensional fitting by using any data distribution. Moreover, the NN is a paradigm that can be realized by using simulation software, analog circuits, optical microsystems and, in the case of this paper, microcontrollers. As discussed in this section, a feed-forward NN (FFNN) with a single hidden layer has been chosen due to reasonable computational cost and its simple structure suitable to be embedded into an inexpensive eight-bit microcontroller. This is in contrast to other effective

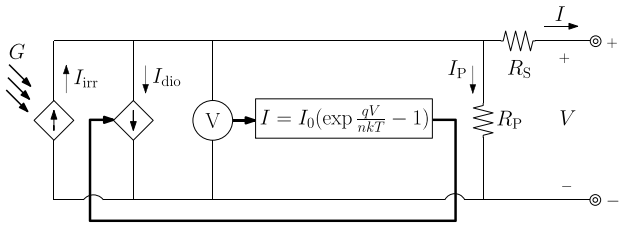

Fig. 4. Equivalent circuit of a PV cell.

TABLE I
SUBSTITUTIONS FOR THE MODEL OF A PV ARRAY

Original Expression	Substitution
$N_{\text{P}} I_{\text{irr}}$	I'_{irr}
$N_{\text{P}} I_0$	I'_0
$\frac{N_{\text{S}}}{N_{\text{P}}} R_{\text{S}}$	R'_{S}
$\frac{N_{\text{S}}}{N_{\text{P}}} R_{\text{P}}$	R'_{P}

NN implementations, such as Bridged Multilayer Perceptron (BMLP) or fully connected cascade (FCC) architectures [29]. Both BMLP and FCC require the implementation of a more elaborate structure and may bring actual benefits for problems involving a large number of neurons.

A. Preparing the Training-Set

The NN training process and hence the performance of the sensor proposed herein relies on a detailed knowledge of the PV array's I–V performance curves for different irradiance and temperature values, such as those illustrated in Figs. 1 and 2, respectively. Performance I–V curves for PV cells can be obtained using their mathematical model along with standard information provided by manufacturer's datasheets. Alternatively, operating points may be experimentally generated in the laboratory under controlled environmental conditions. In either case, a suitable training-set must be constructed by using N different I–V curves depending on the irradiance using a constant temperature. Likewise, M different I–V curves must be obtained by varying the temperature at a constant irradiance. Thus, $N \times M$ training-set patterns must be created. This section provides a detailed description of I–V curves' generation from manufacturer's datasheets and an overview on the experimental synthesis.

1) Generating the Training-Set Using the PV Array Mathematical Model: The circuital model for a single PV cell and its generalization to a number of cells in series is well established in terms of a current source, an anti-parallel diode, a series resistance and shunt resistance [7]. This paper makes use of a modified circuit, which replaces the anti-parallel diode by an external control current source as illustrated in Fig. 4 [30]. A chief advantage of this model is that it allows for including an arbitrary number of cells connected in series and/or parallel into a single circuital representation including all details of each cell. This model corresponds to the building block to generate performance I–V utilized to train the NN.

The output current of the PV cell of Fig. 4 may be expressed as

$$I = I_{\text{irr}} - I_{\text{dio}} - I_p \tag{1}$$

where I_{irr} is the photo current or irradiance current, which is generated when the cell is exposed to sunlight. I_{dio} is the current flowing through the anti-parallel diode, which induces the nonlinear characteristics of the PV cell. I_p is a shunt current due to the shunt resistor R_P branch. Substituting relevant expressions for I_{dio} and I_p

$$I = I_{\text{irr}} - I_0 \left[\exp\left(\frac{q(V + IR_S)}{nkT} \right) - 1 \right] - \frac{V + IR_S}{R_P} \tag{2}$$

where $q = 1.602 \times 10^{-19}$ C is the electron's electric charge, $k = 1.3806503 \times 10^{-23}$ J/K is the Boltzmann constant, T is the temperature of the cell, I_0 is the diode saturation current or cell reverse saturation current, n is the ideality factor or the ideal constant of the diode, and R_S and R_P represent the series and shunt resistance, respectively [7].

This model can be generalized to an arbitrary number of cells connected in series, say N_S, and in parallel, say N_P, to form a small array of $N_S \times N_P$ cells. This may be needed to match voltage/current levels needed by the microcontroller. The generalized model takes the form of

$$I = I'_{\text{irr}} - I'_0 \left[\exp\left(\frac{q(V + IR'_S)}{N_{\text{S}} nkT} \right) - 1 \right] - \frac{V + IR'_S}{R'_P} \tag{3}$$

where the various "prime" values ought to be interpreted according to Table I.

In the I–V performance characteristic of a single PV cell and an array described by (2) and (3), respectively, the parameters I_{irr}, I_0, R_P, R_S, and n depend on the solar irradiance (G), the cell temperature (T), and certain reference parameters, namely G_{ref}, T_{ref}, $I_{\text{irr,ref}}$, $I_{0,\text{ref}}$, $R_{P,\text{ref}}$, $R_{S,\text{ref}}$, and n_{ref}, as described by (4) through (8)

$$I_{\text{irr}} = I_{\text{irr,ref}} \frac{G}{G_{\text{ref}}} (1 + \alpha'_T (T - T_{\text{ref}})) \tag{4}$$

$$I_0 = I_{0,\text{ref}} \left(\frac{T}{T_{\text{ref}}} \right)^3 \exp\left(\frac{E_{\text{g,ref}}}{kT_{\text{ref}}} - \frac{E_{\text{g}}}{kT} \right) \tag{5}$$

$$R_P = R_{P,\text{ref}} \left(\frac{G}{G_{\text{ref}}} \right) \tag{6}$$

$$R_{\text{S}} = R_{S,\text{ref}} \tag{7}$$

$$n = n_{\text{ref}}. \tag{8}$$

In (4), α'_T is the relative temperature coefficient of the short-circuit current, which represents the rate of change of the short-circuit current with respect to temperature. Manufacturers occasionally provide the absolute temperature coefficient of the short-circuit current, α_T, for a particular panel. The relationship between α'_T and α_T is

$$\alpha_T = \alpha'_T I_{\text{irr,ref}}. \tag{9}$$

In (5), E_{g} is the bandgap energy for silicon in eV. Analytical expressions for E_{g} are obtained through curve fitting from

experimental measurements and varies from author to author. Herein the expression from [31] is used

$$E_g = 1.17 - 4.73 \times 10^{-4} \times \frac{T^2}{T + 636}. \tag{10}$$

The I–V equation described by (3) plus the breakdown of the various constituent parameters described by (4) through (8) provide a detailed representation for the performance of an array of an arbitrary size and may be used to train the NN. The reference parameters are PV-cell-specific and may be obtained from information available on manufacturers's datasheets following the methodology outlined in [30].

2) Generating the Training-Set Through Experimental Synthesis: Operating points making up the training-set can alternatively be generated in the laboratory under controlled environmental conditions. The sensing PV cell can be exposed to an adjustable controlled irradiance level and the PV cell loaded at various levels—for example, through using a rheostat—followed by direct measurement of the PV array output voltage and current and cell temperature. This methodology may overcome inaccuracies stemming from: 1) parasitic elements existing on the circuital realization of the proposed sensor; 2) differences between the PV array's datasheet and the actual PV array being used; and 3) tolerance of the testing resistor [26]–[28].

B. Training Process

The training process is of chief importance when using NNs for applications, which need a high level of accuracy. The various design choices in terms of the size of the hidden layer, size of training sets, training algorithm, etc., are strictly linked to the problem being addressed. This has been widely discussed in the literature—see, for example, [32]–[42] and the references within. However, the authors in [43] have identified a somewhat generic procedure leading to a successful design. In general, training a given NN architecture means finding acceptable matrices of synaptic weights and bias vectors, i.e., solving a nonlinear optimization problem in which choosing a suitable search algorithm determines the performance and accuracy of the NN [34], [44], [45].

A well-trained NN must be able to perform a generalization of new data, avoiding the overtraining phenomenon—an overtrained NN performs well on data belonging to the training set, but poorly on data outside. The accuracy of the generalization is determined by the number of hidden neurons (n_{hn}) and the number of samples in the training set (n_{tr}), as well as by the optimization method employed and its initial conditions. The objective of the training process corresponds to finding suitable n_{hn} and n_{tr} such that the mean squared error (MSE) on the validation set (ε_{ts}) approaches the desired small MSE on the training set ($\varepsilon_{\text{tr}} = f(n_{\text{hn}}, n_{\text{tr}})$). For the FFNN considered in this paper, it is possible to establish a map, which relates these quantities thereby providing the basis for a successful design [43].

The map is illustrated in Fig. 5. As suggested in the figure, four regions are identified: 1) a region defined by $n_{\text{hn}} < n_{\text{hn0}}$, where in practice is impossible to reach the desired ε_{tr} because

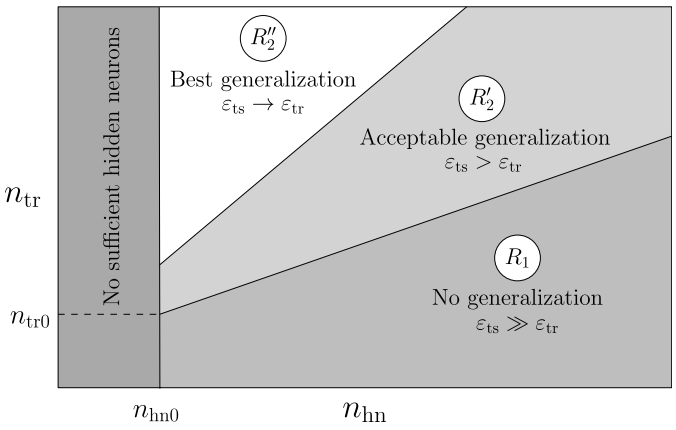

Fig. 5. Map for the training of a FFNN.

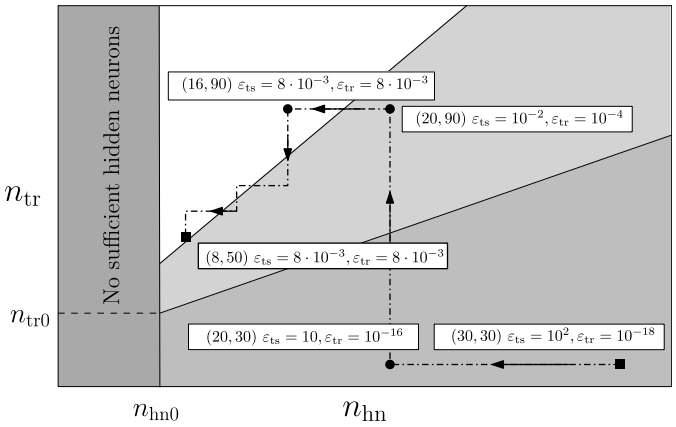

Fig. 6. Learning procedure followed to train the NN.

the number of hidden neurons is less than those required by the problem being addressed (n_{hn0}); 2) a region R_1 where $\varepsilon_{\text{ts}} \gg \varepsilon_{\text{tr}}$ and the FFNN performs no generalization because the training set is too small; 3) a region $R_2^{'}$ where $\varepsilon_{\text{ts}} > \varepsilon_{\text{tr}}$, but ε_{ts} begins to approach the small value of ε_{tr} and an acceptable generalization is achieved; and 4) $R_2^{''}$ where ε_{ts} becomes in practice equal to ε_{tr}, providing the best generalization in terms of adequate n_{hn} and n_{tr}. Consequently, the objective of a successful training is reaching region $R_2^{''}$.

Furthermore, it is important to select a small FFNN so it can be effectively embedded in a modest-memory microcontroller. Hence, the minimum size of the training set to remain in $R_2^{''}$ must be identified. This can be achieved by the iterative procedure described in [43] which, for a given wide validation set, modifies n_{hn} or n_{tr} in order to reach the region $R_2^{''}$ with a desired ε_{tr}.

For the training herein, a target MSE on the training set of $\varepsilon_{\text{tr}} = 8 \times 10^{-3}$ was considered. Starting from a large value of n_{hn}, the iterative process yielded $n_{\text{hn}} = 8$ and $n_{\text{tr}} = 50$ as optimal values to reach the region $R_2^{''}$. A further reduction of the number of neurons provides no useful results. In Fig. 6, the results obtained during the execution of the learning procedure are marked. Each point $(\cdot, \cdot)$ contains the number of neurons and training set size in the first and second entry, respectively. Moreover, the values of the training and validation errors are shown besides the points.

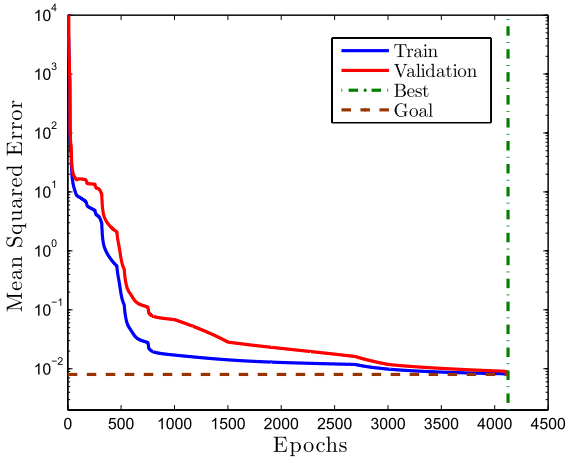

Fig. 7. NN's training and validation processes. Best training performance is 0.0079999 at epoch 4125.

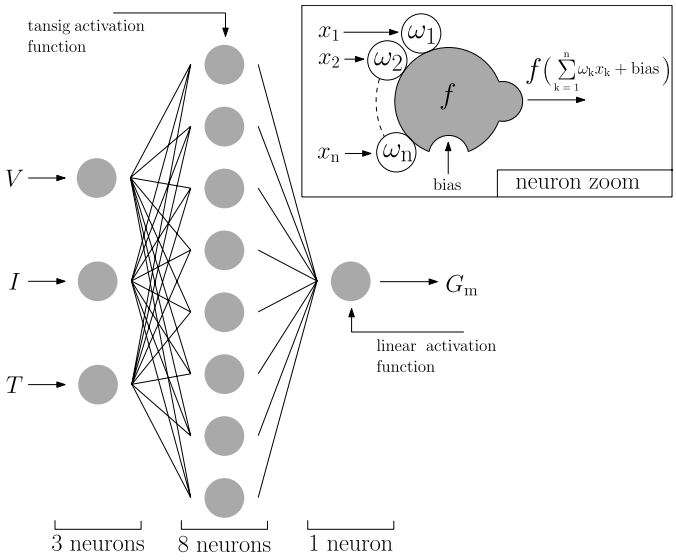

Fig. 8. Architecture of the proposed FFNN scheme.

These results are compatible with the requirements of a FFNN with a low computational cost and reduced employed memory in the microcontroller. As reported in the literature, the choice of the training algorithm can play a relevant role in the training process [34], [43]. For the training implemented in this paper, a hybridization between the well-known Levenberg–Marquardt algorithm (LMA) [46] and a Genetic Algorithm (GA) [43], [45] was utilized.

In summary, the adopted NN has a feed-forward architecture and it is characterized by a three-layer structure with: 1) three input neurons (with linear activation function); 2) eight neurons for the hidden layer with tansig activation function; and 3) one output neuron (with linear activation function) for prediction of the measured irradiance, G_{m}.

The NN's training set was implemented in the MATLAB environment through $N = 10$ different operating points at equidistant irradiance values from 100 to 1500 W/m^2 and $M = 5$ different operating points at equidistant temperature values from 260 to 360 (K), which leads to a training set size of $N \times M = 50$ operating points $[V, I, T]$. The goal for mean square error (MSE) on training set was fixed equal to 8×10^{-3} and the whole learning process took around 2 min. Fig. 7 shows the MSE during the NN training and validation.

After 4125 epochs, the target value for MSE was reached. Some remarks are in order: 1) by following the procedure previously described, there is no risk of overtraining; 2) the slow drop of MSE in Fig. 7 is in part due to the few hidden neurons employed; and 3) since a very large validation set has been utilized—with a wide range of both solar irradiance and cell temperature—it is expected the results on new data will be accurate in every case.

The NN has been trained to return G_{m} from the operating point identified by the voltage (V) and current (I) at the PV cell terminals and the temperature on the PV cell surface (T). The trio $x = [V, I, T]$ corresponds to the NN's input vector. It is important to note from the PV cell model described by (2) or (3) plus (4) through (8) that a one-to-one relationship exists between the operating points x and the single values of G. Furthermore, in the hardware implementation, only V and T have to be measured. Indeed, direct measurement of I is avoided through using a known testing resistor, R_{test}, so the current I can be computed using Ohm's Law. In order to improve accuracy and make the various numerical processes more robust, the value of R_{test} ought to be selected so that most of the operating points lie around the elbow of the PV cell's I–V curves, thus benefiting from a greater range of values for all three variables $[V, I, T]$.

C. Irradiance Computation

The training process returns the matrices of synaptic weights W_1 and W_2 and bias vectors B_1 and B_2 for the hidden and output layer, respectively. The measured irradiance G_{m} is computed through the following three-step procedure.

1) Scaling operation (Min–Max normalization) of the input data, according to the formulas

$$x_j^n = \frac{x_j - x_j^{\min}}{x_j^{\max} - x_j^{\min}} \quad \text{for} \quad j = 1, 2, 3 \tag{11}$$

where x_j corresponds to V, I and T for $j = 1$, 2, and 3, respectively, $x_j^{\max}$ and $x_j^{\min}$ are the maximum and minimum values of V, I and T, and x_j^n is the normalized input value within the range $[-1\ 1]$.

2) Computation of the scaled irradiance

$$G_n = W_2 \times \mathrm{tansig}(W_1 \times x^n + B_1) + B_2 \tag{12}$$

where the activation function tansig is

$$\mathrm{tansig}(A) = \frac{2}{1 + e^{-2A}} - 1. \tag{13}$$

3) De-scaling of G_n in order to obtain the actual solar irradiance value

$$G_m = (G^{\max} - G^{\min})G_n + G^{\min}. \tag{14}$$

The computation sequence is further explained through the schematic of Fig. 8, where a neuron zoom is also included.

D. Hardware Implementation

The circuit schematic of Fig. 3 was prototyped in the laboratory for experimental validation. The sensing PV array was realized by a prepackaged eight-cell array manufactured by IXYS, part # KXOB22-01X8, rated at 3.4 V/3.8 mA at MPP under standard testing conditions [47]. Using the specifications available on the manufacturer's datasheet, a complete mathematical model for the performance of the array was built using the procedure outlined in Section III-A.1.

Given the PV array characteristics, the resistance of the testing resistor was selected to be $R_{\text{test}} = 921\ \Omega$ and was realized through a simple axial-lead resistor. This allows one to select operating points around the elbow of the PV array I–V curve. The PV array terminal voltage is measured using an internal analog/digital (AD) converter embedded in the microcontroller.

The temperature sensor was realized using a one-wire sensor Maxim Integrated model # DS18B20. The microcontroller used for data processing is a PIC18F6627 manufactured by Microchip Technology Inc. This device belongs to the low-cost low-power PIC18/8-bit family, featuring a 4 kB RAM memory and a 96 kB reprogrammable flash memory; 12 AD converters; and SPI, I2C, and RS232/RS485 interfaces.

The selection of an inexpensive microcontroller is essential for a low-cost implementation of the proposed sensor. This inevitably makes an eight-bit microcontroller the device of choice for the implementation, which comes at a cost of possible numerical errors. Fortunately, there are now accurate double-precision mathematic libraries, which are available for the development of the firmware of microcontrollers. The NN algorithm described in Section III-C has been adapted to run in the microcontroller, and coded in C language. The C code consists of a set of initializing functions and a main process. The latter controls the peripheral units, manages the communication protocols, acquires the input data, executes the implemented NN routine, and outputs the computed irradiance. The routines for control and communication processes are readily available on the Microchip website [48]. They are developed by means of the MPLAB X IDE and compiled through the Microchip C 18 compiler. This restitutes a HEX code file, which is downloaded into the microcontroller via Ethernet connection. Furthermore, the microcontroller can be interfaced to a personal computer through a RS232/RS485 or an Ethernet cable. The aforementioned features of the microcontroller allows for easy updates, recalibration, or the inclusion of new customized features. The entire NN routine occupies just 5904 bytes of program memory and 186 bytes of data memory. The microcontroller accuracy was contrasted against results computed using MATLAB and no remarkable difference was observed.

Table II shows the cost of the main components for the hardware realization as listed on the Digi-Key website [49]. Although the cost of a commercial product based in the sensor proposed herein is a complex function of market trends, economic factors, and engineering development, the components cost of about USD $40–50 makes the sensor at least competitive with inexpensive irradiance sensors existing in the market. Dedicated components in a mass production setting may further reduce the price of the sensor.

TABLE II
EXPERIMENTAL SETUP COMPONENTS AND COST

Component	Off–the–shelf part #	Cost (USD $)
PV cell	KXOB22–01X8	5.8
Temperature Sensor	DS18B20	4.5
Microcontroller	PIC18F6627	11.0
Other components	Connectors, case, etc.	20.0/30.0
	Total cost =	**41.3/51.3**

Fig. 9. Photo of the outdoor measurement setup showing the developed prototype and commercial sensor.

IV. EXPERIMENTAL VERIFICATION

Outdoor experiments were performed using the hardware prototype described in Section III-D on the roof of the North Classroom building at the University of Colorado Denver campus. The proposed sensor was contrasted against a commercial sensor. The device available for comparison is a laser power sensor part # LM-10 HTD manufactured by Coherent, Inc., [50]. The photo in Fig. 9 shows the experimental setup and a closeup of the prototype and the commercial sensor.

The PV cells utilized in the sensor realization proposed herein corresponds to a monocrystalline silicon cell pack, which absorb light within the wavelength range 0.3–1.1 μm [47]. On the other hand, the LM-10 HTD device is a thermopile-based sensor. It is calibrated to measure irradiance within the spectrum 0.25–10.6 μm [50].

It is well documented in the literature that, because of the mismatch in the wavelength spectrum, monocrystalline silicon cell- and thermopile-based sensors do not yield same readings [51]–[54]. The authors in [51] developed experimental procedures to quantify these differences through the definition of mismatch ratio (MR). In the case of irradiance measured by a sensor based on monocrystalline silicon cells (G_{Pv}) versus one based on a thermopile (G_{Tp}), the mismatch ratio ($\text{MR} = G_{\text{Pv}}/G_{\text{Tp}}$) is 0.946. This correction was applied to the outdoor measurements in order to compare the sensors' readings. Data per comparison was collected November 11, 2012 at

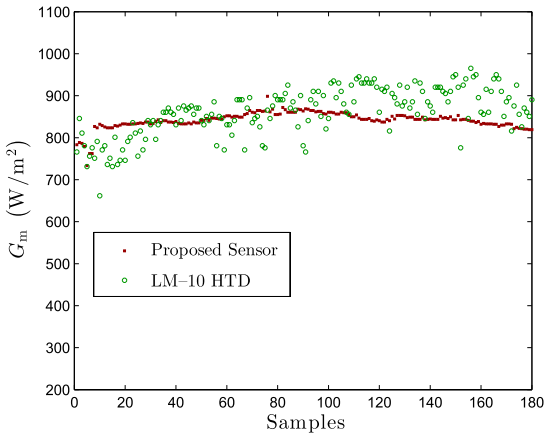

Fig. 10. Solar irradiance values measured by the proposed sensor and the commercial device LM-10 HTD. Samples taken from 12:20 p.m. to 1:50 p.m. every 30 s, illustrating a period of relatively constant irradiance.

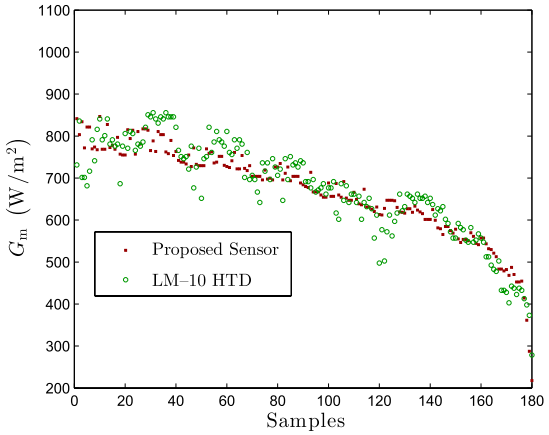

Fig. 11. Solar irradiance values measured by the proposed sensor and the commercial device LM-10 HTD. Samples taken from 2:50 p.m. to 4:20 p.m. every 30 s, illustrating a period of changing irradiance.

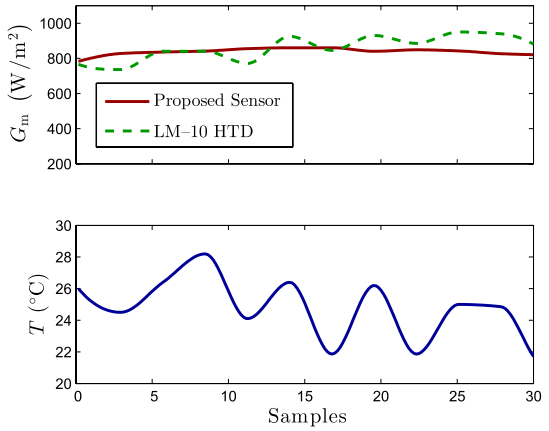

Fig. 12. Solar irradiance and temperature trends extracted by resampling the measured data of Fig. 10 every 3 min.

a time of relatively constant irradiance around noon (Fig. 10) and at a period of rapidly changing irradiance during dusk (Fig. 11). The correlation among the readings is evident.

Furthermore, Figs. 12 and 13 present the same data as those of Figs. 10 and 11, respectively, resample every 3 min and

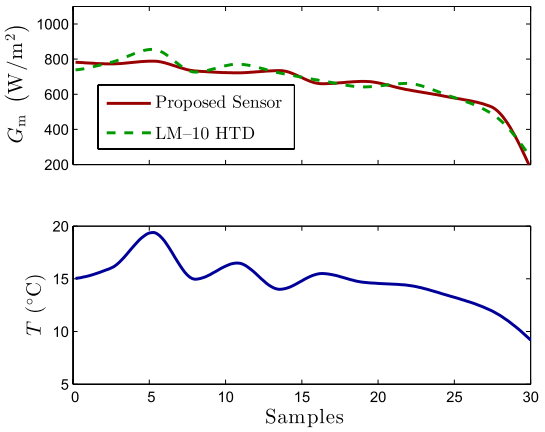

Fig. 13. Solar irradiance and temperature trends extracted by resampling the measured data of Fig. 11 every 3 min.

plotted using a linear fit. Temperature readings are also shown in the bottom plot in the figures. As the figures suggest, the irradiance readings in the LM-10 HTD sensor—designed for indoor laser power measurements in the absence of wind—are affected by fluctuations in the temperature due to the wind, while the NN sensor proposed herein is insensitive to these.

V. Conclusion

This paper has introduced a novel low-cost NN-based solar irradiance sensor conceived to be utilized in large PV power plants for precise tracking of solar irradiance within the PV power plant layout. A complete mathematical model as well as a practical realization of the sensor has been described in detail, and outdoor measurements have been used to validate the sensor. An important feature of the approach proposed herein lies in the simplicity of construction along with a high degree of accuracy, thanks to the use of a NN implemented in a embedded system through a microcontroller.

The NN was implemented through a simple feed-forward architecture with a single hidden layer. The selection of this architecture was motivated by its reasonable computational cost and simple structure suitable to be embedded into an inexpensive eight-bit microcontroller. An interesting area of further research could be a comparison among different types of NNs as an evolution of this paper.

The use of a microcontroller allows for updates, enhancement, and customization by simply adding code libraries. Moreover, it can be interfaced via RS232 or RS485 with other instruments or connected via Ethernet and remote controlled through its embedded web server. A chief advantage of this sensor is that it can be conveniently located next to a power-producing PV panel or even integrated with it. As a result, the sensing PV panel will "see" exactly the same solar irradiance and temperature as what is "seen" by the power-producing PV panel, leading to precise irradiance tracking thereby improving MPPT performance.

REFERENCES

[1] S. Kuszamaul, A. Ellis, J. Stein, and L. Johnson, "Lanai high-density irradiance sensor network for characterizing solar resource variability of MW-scale PV system," in *Proc. 35th IEEE Photovolt. Specialists Conf.*, Jun. 2010, pp. 283–288.

[2] M. Shams El-Dein, M. Kazerani, and M. M. A. Salama, "Optimal photovoltaic array reconfiguration to maximize power production under partial shading," in *Proc. 11th Int. Conf. Environ. Electr. Eng.*, May 2012, pp. 255–260.

[3] T. Hiyama and K. Kitabayashi, "Neural network based estimation of maximum power generation from PV module using environmental information," *IEEE Trans. Energy Convers.*, vol. 12, no. 3, pp. 241–247, Sep. 1997.

[4] D. R. Myers, "Solar radiation modeling and measurements for renewable energy applications: Data and model quality," *Energy*, vol. 30, no. 9, pp. 1517–1531, Jul. 2005.

[5] R. Kadri, J. P. Gaubert, and G. Champenois, "An improved maximum power point tracking for photovoltaic grid-connected inverter based on voltage-oriented control," *IEEE Trans. Ind. Electron.*, vol. 58, no. 1, pp. 66–75, Jan. 2011.

[6] F. Mancilla-David, A. Arancibia, F. Riganti-Fulginei, E. Muljadi, and M. Cerroni, "A maximum power point tracker variable-dc-link three-phase inverter for grid-connected PV panels," in *Proc. IEEE PES Innovative Smart Grid Technol.*, Oct. 2012, pp. 1–7.

[7] G. M. Masters, *Renewable and Efficient Electric Power Systems*. New York, NY, USA: Wiley, 2004.

[8] W. Lin, C. Hong, and C. Chen, "Neural-network-based MPPT control of a stand-alone hybrid power generation system," *IEEE Trans. Power Electron.*, vol. 26, no. 12, pp. 3571–3581, Dec. 2011.

[9] A. Chatterjee and A. Keyhani, "Neural network estimation of microgrid maximum solar power," *IEEE Trans. Smart Grid*, vol. 3, no. 4, pp. 1860–1866, Dec. 2012.

[10] Syafaruddin, E. Karatepe, and T. Hiyama, "Artificial neural network-polar coordinated fuzzy controller based maximum power point tracking control under partially shaded conditions," *IET Renew. Power Generat.*, vol. 3, no. 2, pp. 239–253, Jun. 2009.

[11] M. Goncalves Wanzeller, R. N. C. Alves, J. da Fonseca Neto, and W. A. S. Fonseca, "Current control loop for tracking of maximum power point supplied for photovoltaic array," *IEEE Trans. Instrum. Meas.*, vol. 53, no. 4, pp. 1304–1310, Aug. 2004.

[12] G. Velasco-Quesada, F. Guinjoan-Gispert, R. Pique-Lopez, M. Roman-Lumbreras, and A. Conesa-Roca, "Electrical PV array reconfiguration strategy for energy extraction improvement in grid-connected PV systems," *IEEE Trans. Ind. Electron.*, vol. 56, no. 11, pp. 4319–4331, Nov. 2009.

[13] N. Zhang and P. K. Behera, "Solar radiation prediction based on recurrent neural networks trained by Levenberg-Marquardt backpropagation learning algorithm," in *Proc. IEEE PES Innovative Smart Grid Technol.*, Jan. 2012, pp. 1–7.

[14] J. Yeom, K. Han, Y. Park, C. Lee, and Y. Kim, "A improvement for the surface solar insolation retrieval from geostationary sensor," in *Proc. IEEE Int. Geosci. Remote Sens. Symp.*, Jul. 2007, pp. 1689–1692.

[15] L. Cristaldi, M. Faifer, M. Rossi, and F. Ponci, "A simple photovoltaic panel model: Characterization procedure and evaluation of the role of environmental measurements," *IEEE Trans. Instrum. Meas.*, vol. 61, no. 10, pp. 2632–2641, Oct. 2012.

[16] J. Cruz-Colon, L. Martinez-Mitjans, and E. I. Ortiz-Rivera, "Design of a low cost irradiance meter using a photovoltaic panel," in *Proc. 38th IEEE Photovolt. Specialists Conf.*, Jun. 2012, pp. 2911–2912.

[17] N. S. Husain, N. A. Zainal, B. S. Mahinder Singh, N. M. Mohamed, and N. Mohd Nor, "Integrated PV based solar insolation measurement and performance monitoring system," in *Proc. IEEE Colloq. Humanities, Sci. Eng.*, Dec. 2011, pp. 710–715.

[18] L. S. Saoud and A. Khellaf, "A neural network based on an inexpensive eight-bit microcontroller," *Neural Comput. Appl.*, vol. 20, no. 3, pp. 329–334, Apr. 2011.

[19] B. M. Wilamowski, "Suitability of fuzzy systems and neural networks for industrial applications," in *Proc. 13th Int. Conf. Optim. Electr. Electron. Equip.*, May 2012, pp. 1–7.

[20] J. Ibanez Civera, E. Garcia Breijo, N. Laguarda Miro, L. Sanchez, J. Garrigues Baixauli, I. Romero Gil, R. Masot Peris, and M. Alcaniz Fillol, "Artificial neural network onto eight bit microcontroller for Secchi depth calculation," *Sens. Actuators B, Chem.*, vol. 156, no. 1, pp. 132–139, Aug. 2011.

[21] J. Pelegri-Sebastia, E. Garcia-Breijo, J. Ibanez, T. Sogorb, N. Laguarda-Miro, and J. Garrigues, "Low-cost capacitive humidity sensor for application within flexible rfid labels based on microcontroller systems," *IEEE Trans. Instrum. Meas.*, vol. 61, no. 2, pp. 545–553, Feb. 2012.

[22] U. Farooq, M. Amar, E. Ul Haq, M. U. Asad, and H. M. Atiq, "Microcontroller based neural network controlled low cost autonomous vehicle," in *Proc. 2nd Int. Conf. Mach. Learn. Comput.*, 2010, pp. 96–100.

[23] R. Mukaro and X. F. Carelse, "A microcontroller-based data acquisition system for solar radiation and environmental monitoring," *IEEE Trans. Instrum. Meas.*, vol. 48, no. 6, pp. 1232–1238, Dec. 1999.

[24] N. J. Cotton, B. M. Wilamowski, and G. Dundar, "A neural network implementation on an inexpensive eight bit microcontroller," in *Proc. 12th Int. Conf. Intell. Eng. Syst.*, 2008, pp. 109–114.

[25] F. Attivissimo, A. Di Nisio, M. Savino, and M. Spadavecchia, "Uncertainty analysis in photovoltaic cell parameter estimation," *IEEE Trans. Instrum. Meas.*, vol. 61, no. 5, pp. 1334–1342, May 2012.

[26] A. Carullo and A. Vallan, "Outdoor experimental laboratory for long-term estimation of photovoltaic-plant performance," *IEEE Trans. Instrum. Meas.*, vol. 61, no. 5, pp. 1307–1314, May 2012.

[27] F. Adamo, F. Attivissimo, A. Di Nisio, and M. Spadavecchia, "Characterization and testing of a tool for photovoltaic panel modeling," *IEEE Trans. Instrum. Meas.*, vol. 60, no. 5, pp. 1613–1622, May 2011.

[28] H. Andrei, T. Ivanovici, E. Diaconu, M. R. Ghita, O. Marin, and P. C. Andrei, "Analysis and experimental verification of the sensitivity of PV cell model parameters," in *Proc. Int. Conf. Synth., Model., Anal. Simul. Methods Appl. Circuit Design*, Sep. 2012, pp. 129–132.

[29] J. Binfet and B. Wilamowski, "Microprocessor implementation of fuzzy systems and neural networks," in *Proc. IJCNN*, vol. 1. 2001, pp. 234–239.

[30] H. Tian, F. Mancilla-David, K. Ellis, E. Muljadi, and P. Jenkins, "A cell-to-module-to-array detailed model for photovoltaic panels," *Solar Energy*, vol. 86, no. 9, pp. 2695–2706, Sep. 2012.

[31] R. F. Pierret, *Semiconductor Device Fundamentals*. Lebanon, IN, USA: Addison-Wesley, 1996.

[32] F. Riganti-Fulginei and A. Salvini, "Neural network approach for modelling hysteretic magnetic materials under distorted excitations," *IEEE Trans. Magn.*, vol. 48, no. 2, pp. 307–310, Feb. 2012.

[33] F. Riganti-Fulginei, A. Salvini, and M. Parodi, "Learning optimization of neural networks used for MIMO applications based on multivariate functions decomposition," *Inverse Problems Sci. Eng.*, vol. 20, no. 1, pp. 29–39, 2012.

[34] B. Wilamowski, "Neural network architectures and learning algorithms," *IEEE Ind. Electron. Mag.*, vol. 3, no. 4, pp. 56–63, Dec. 2009.

[35] W. Xie, Y. Zhu, Z. Zhao, and Y. Wong, "Nonlinear system identification using optimized dynamic neural network," *Neurocomputing*, vol. 72, no. 13–15, pp. 3277–3287, Aug. 2009.

[36] R.-M. Chen, "Reducing network and computation complexities in neural based real-time scheduling scheme," *Appl. Math. Comput.*, vol. 217, no. 13, pp. 6379–6389, Mar. 2011.

[37] L. dos Santos Coelho and M. W. Pessôa, "Nonlinear identification using a B-spline neural network and chaotic immune approaches," *Mech. Syst. Signal Process.*, vol. 23, no. 8, pp. 2418–2434, Nov. 2009.

[38] H.-W. Ge, W.-L. Du, F. Qian, and Y.-C. Liang, "Identification and control of nonlinear systems by a time-delay recurrent neural network," *Neurocomputing*, vol. 72, nos. 13–15, pp. 2857–2864, Aug. 2009.

[39] B. Majhi and G. Panda, "Robust identification of nonlinear complex systems using low complexity ANN and particle swarm optimization technique," *Expert Syst. Appl.*, vol. 38, no. 1, pp. 321–333, Jan. 2011.

[40] H. M. R. Ugalde, J. Carmona, V. M. Alvarado, and J. Reyes-Reyes, "Neural network design and model reduction approach for black box nonlinear system identification with reduced number of parameters," *Neurocomputing*, vol. 101, no. 4, pp. 170–180, Feb. 2013.

[41] H. M. R. Ugalde, J. Carmona, and V. M. Alvarado, "1/2 nonlinear system identification: A balanced accuracy/complexity neural network approach," in *Proc. 2nd Int. Conf. CCCA*, 2012, pp. 1–6.

[42] H. M. R. Ugalde, J. Carmona, and V. M. Alvarado, "2/2 training time optimization for balanced accuracy/complexity neural network models," in *Proc. 2nd Int. Conf. CCCA*, 2012, pp. 1–6.

[43] F. Riganti-Fulginei, A. Laudani, A. Salvini, and M. Parodi, "Automatic and parallel optimized learning for neural networks performing MIMO applications," *Adv. Electr. Comput. Eng.*, vol. 13, no. 1, pp. 3–12, 2013.

[44] D. H. Wolpert and W. G. Macready, "No free lunch theorems for optimization," *IEEE Trans. Evol. Comput.*, vol. 48, no. 2, pp. 307–310, Apr. 1997.

[45] F. Riganti-Fulginei and A. Salvini, "Comparative analysis between modern heuristics and hybrid algorithms," *Int. J. Comput. Math. Electr. Electron. Eng.*, vol. 26, no. 2, pp. 259–268, 2007.
[46] P. R. Gill, W. Murray, and M. H. Wright, *Practical Optimization*. London, U.K.: Academic, 1981.
[47] (2013). IXYS. Milpitas, CA, USA [Online]. Available: http://ixapps.ixys.com/DataSheet/KXOB22-01X8-DATA-SHEET-20110818-.pdf
[48] (2013). Microchip. Chandler, AZ, USA [Online]. Available: http://www.microchip.com/
[49] (2013). Digi-Key Corporation. Thief River Falls, MN, USA [Online]. Available: http://www.digikey.com/
[50] (2013). Coherent Inc. Santa Clara, CA, USA [Online]. Available: http://www.coherent.com
[51] B. Schulz, T. Glotzbach, C. Vodermayer, G. Wotruba, M. Mayer, and S. Grünsteidl, "Evaluation of calibrated solar cells and pyranometers regarding the effective irradiance detected by PV modules," in *Proc. 25th Eur. Photovolt. Solar Energy Conf., Exhibit./5th World Conf. Photovolt. Energy Convers.*, Oct. 2012, pp. 4797–4800.
[52] N. Van der Borg and E. J. Wiggelinkhuizen, "Irradiation loss in the built environment," in *Proc. 17th Eur. Photovolt. Solar Energy Conf.*, Oct. 2001, pp. 1–4.
[53] D. R. Myers, "Silicon cell pyranometers: The cost of accuracy," *Solar Spectrum*, vol. 11, no. 2, pp. 1–5, Nov. 1998.
[54] A. Raïch, J. A. González, and J. Calbó, "Effects of solar height, cloudiness and temperature on silicon pyranometer measurements," *Tethys, J. Medit. Meteorol. Climatol.*, vol. 4, pp. 11–18, Apr. 2007.

Fernando Mancilla-David (S'05–M'07) received the B.S. degree in electrical engineering from the Universidad Técnica Federico Santa María, Valparaíso, Chile, in 1999, and the M.S. and Ph.D. degrees in electrical engineering from the University of Wisconsin-Madison, Madison, Wisconsin, in 2002 and 2007, respectively.

Currently, he is an Assistant Professor at the University of Colorado Denver in Denver, CO, USA. He was a visiting scientist at ABB Corpo Research in Västerås, Sweden in the summer of 2008, and has held visiting professor positions at L'Ecole supérieure d'électricité (Supélec) in Gif-sur-Yvette, France, in the summers of 2009 and 2010, at the Technische Universität Berlin, Berlin, Germany, in the summer of 2011, and at the Università Degli Studi Roma Tre, Rome, Italy in the summer of 2012. His research interests are power system analysis, energy systems, utility applications of power electronics, control systems, and optimization problems.

Francesco Riganti-Fulginei (M'12) is an Assistant Professor at the University of Roma Tre, Rome, Italy, where he teaches and directs research in non-linear optimization and inverse problems as a faculty member of the Department of Applied Electronics. Prof. Riganti-Fulginei received the Ph.D. degree in biomedical electronics, electromagnetism and telecommunications engineering at the University of Roma Tre in 2007. He is the author of several international publications and has been a visiting professor at the University of Colorado Denver, Denver, CO, USA and Okayama University, Okayama, Japan. His research interests include non-linear optimization and inverse problems applied to complex systems, in particular power electronics and electromagnetic devices.

Antonino Laudani (M'09) was born in Catania, Italy, in 1973. He received the Laurea degree (*Cum Laude*) from the University of Catania, Italy, in 1999 and the Ph.D. degree from the University of Reggio Calabria, Italy in 2003, both in Electronic Engineering.

Currently, he is an Assistant Professor of Electrotechnics in the Department of Applied Electronics at the University of Roma Tre. He is the author of more than 70 international publications. His main research interests include finite elements computation of electromagnetic fields, particle in cell methods, innovative techniques for the postprocessing of numerical solutions, neural networks, optimization and inverse problem solutions, and in the design of embedded system.

Alessandro Salvini (M'02) received the Laurea degree in Electrical Engineering (*Cum Laude*) from the University of Rome La Sapienza.

He was an Assistant Professor (1994), an Associate Professor (2001) and, at the present, he is a Full Professor at the University of Roma Tre, where he is also the Scientific Coordinator of the Research Unit of Electrical Engineering. He is involved in tutoring Ph.D. students and is responsible for international agreements with foreign universities for the exchange of faculty and students. His research interests include magnetic material modeling, dynamic hysteresis, optimization and inverse problems, soft computing, and evolutionary computation.